Effects of Polydispersity on Phase Behavior of Diblock Copolymers

David M. Cooke[†] and An-Chang Shi*

Department of Physics and Astronomy, McMaster University, Hamilton, Ontario, Canada L8S 4M1

Received March 30, 2006; Revised Manuscript Received July 20, 2006

ABSTRACT: The influence of polydispersity on the phase behavior of diblock copolymer melts is studied using a self-consistent field theoretic model. A perturbation theory is developed for the polydisperse system, in which the polydispersity index, $\kappa = M_w/M_n - 1$, is taken as a perturbation parameter. Phase diagrams are constructed using the reciprocal space method. It is found that the order−disorder transition boundary shifts to higher temperatures, as predicted by a random phase approximation analysis. For asymmetric polymer distributions, polydispersity favors structures with curved interfaces. The domain spacing of the ordered structures increases with increasing polydispersity index. An analysis of the free energy provides an understanding of the mechanism of these effects.

Introduction

Block copolymers are macromolecules formed by chemically linking different polymer chains together. The self-assembly of block copolymers is governed by a delicate balance of the interaction energy and the chain stretching. The repulsive interaction between the chemically different blocks drives the system to phase separation, whereas the connectivity of the copolymer chains prevents macroscopic phase separation. As a result of these competing trends, block copolymer systems self-organize into many complex structures.[1] For the simplest case of diblock coplymers (linear polymer chains composed of two different blocks), the phase behavior is well established. A variety of ordered phases, including a lamellar structure (L), hexagonally packed cylinders (C), body-centered-cubic spheres (S), and a bicontinuous network structure called the gyroid (G), are observed.[2] These structures can be controlled by varying the chemical composition of the block copolymer or the segregation between blocks (via temperature or molecular weight). The composition of an AB diblock copolymer is characterized by the volume faction of the A-blocks f_A. The extent of segregation can be expressed using the reduced parameter χN, where χ is the Flory−Huggins interaction parameter, and N is the copolymer degree of polymerization. At small values of χN, the copolymer melts assume a disordered state. The transition from a homogeneous melt of chains to a heterogeneous melt of ordered structure occurs at the order−disorder transition (ODT). This transition corresponds to a critical value of χN and depends on the composition of the copolymer f_A, which in turn determines the spontaneous curvature of the interface between the blocks. For the ordered phases, the equilibrium morphology adopted by the AB diblock copolymers depends on the volume fraction of the A component (f_A) and the degree of segregation between the two blocks (χN).[3]

Because of their importance, a variety of theoretical approaches have been used to investigate the phase behavior of block copolymers.[4] Among the different theoretical approaches, the self-consistent field theory (SCFT) provides a powerful tool for the study of ordered phases of block copolymers.[5] SCFT is a coarse-grained field theory in which the polymer densities are the primary variables. The theory has its origin from the field theoretical approach of Edwards in the 1960s.[6] Helfand and others explicitly adopted the theory to the study of block copolymer phase behavior.[7] In recent years, SCFT has developed into a powerful tool to study block copolymer self-assembly. For the bulk ordered phases, Matsen and Schick[8] have successfully solved the SCFT equations numerically, using a restricted Fourier basis which was selected on the basis of the assumed morphological symmetries. The Matsen-Schick approach is efficient, and it allows accurate calculations of the free energies, which are used to construct phase diagrams for the block copolymer systems. This reciprocal-space method is complemented by real-space methods, which solve the SCFT equations in real space. In particular, Drolet and Fredrickson[9] suggested an implementation where low free energy morphologies are found by relaxation from random potential fields. A similar real-space approach has also been suggested by Bohbot-Raviv and Wang.[10]

In most of the theoretical approaches, the polymers are assumed to be monodisperse; i.e., all of the chains are of the same length. However, all synthetic polymers are polydisperse, characterized by a molecular weight distribution which is often parametrized using the polydispersity index (PDI $= M_w/M_n$, where M_w is the weight-averaged molecular weight, and M_n is the number-averaged weight). It is well-known that many of the unique static and dynamic properties of polymers depend on chain length and it is expected that polydispersity will influence those properties. It is, therefore, important to study the influence of the molecular weight distribution on the phase behavior of block copolymers. A number of theoretical studies incorporating polydispersity into block copolymer models have appeared in the literature. Leibler and Benoit[11] and Hong and Noolandi[12] have performed random-phase approximation (RPA) studies for disordered block copolymer melts using a continuous Schulz−Zimm distribution for the molecular weight distributions. These studies assumed that there is only one chain-length distribution, that of the total polymer, and the A and B blocks of each polymer chain are in a constant fraction to each other. In reality, the two blocks would be grown separately, and any given polymer will not have the same fraction of A to B as the average. In a related study, Burger and co-workers[13] studied the ordered phase structures of polydisperse diblock copolymers using an extension of the weak segregation theory, along with a RPA analysis using independent block distributions. Continu-

* Corresponding author. E-mail: shi@physics.mcmaster.ca.
[†] E-mail: cookedm@physics.mcmaster.ca.

10.1021/ma060717s CCC: $33.50
Published on Web 08/19/2006

ous thermodynamics was used by Spontak and Williams to examine polydisperse poly(styrene−butadiene) diblock (SB) and triblock (SBS) copolymers.[27] In particular, they examined the critical molecular weight for microphase phase separation and the interphase thickness. In a series of papers,[28] Birshtein, Liatskaya, and Zhulina used the narrow interface approximation to study the strong-segregation limit of polydisperse diblock copolymers, although most of their results are for a bidisperse mixture. Recently Fredrickson and Sides have proposed an efficient SCFT method to study the effect of polydispersity on the bulk phase behavior of block copolymer melts.[14,15] They extended the SCFT to include polydispersity and used a Gaussian quadrature method to carry out the integrals over the molecular weight distributions. The SCFT equations were solved in real-space. The computations were carried out for a model system in which one block is assumed to be monodisperse. The studies show that an increasing PDI leads to a larger domain spacing, and the molecular weight distribution could dramatically affect the phase behavior of block copolymers.

Because of the difficulty of synthesizing block copolymers with a well-controlled molecular weight distribution, there have been a few systematic experimental studies on polydispersity effects on block copolymer phase behavior. Matsushita and coworkers[16,17] synthesized a series of polystyrene-*b*-poly(2-vinylpyridine) diblock copolymers with narrow molecular weight distributions. These copolymers were blended to prepare bimodal and trimodal copolymer systems with different PDI. They observed that the lamellar domain spacing increases as PDI is increased. For PDI > 1.8, macrophase separation was observed. Bendejaq et al.[18] obtained several polystyrene-*b*-poly(acrylic acid) diblock copolymers with broad molecular weight distributions and discovered that these systems produced well-ordered structures. Very recently, Lynd and Hillmyer[19] have synthesized several sets of poly(ethylene-*alt*-propylene)-*b*-poly(DL-lactide) diblock copolymers with controlled molecular weights, compositions and polydispersity indices. Small-angle X-ray scattering was used to evaluate the influence of block copolymer polydispersity on the equilibrium domain spacing and resultant ordered structure. They observed that the domain spacing increases linearly with increasing polydispersity for PDI from 1.20 to 2.00. The experiments also show that larger PDI can lead to a change in morphology for compositionally asymmetric diblock copolymers.

In this paper we study the phase behavior of polydisperse AB diblock copolymer melts using a reciprocal-space SCFT approach. In principle, both blocks of the copolymers can be polydisperse with different molecular weight distributions. The polydispersity is characterized by a continuous molecular weight distribution. In the model, the polydisperse block can be either the A or B blocks. Our theoretical framework is similar to the SCFT for polydisperse melts developed by Fredrickson and Sides. The real-space approach adopted by Fredrickson and Sides[14,15] is an excellent tool to explore different structures, while the reciprocal-space approach adopted here provides accurate calculation of the free energies of the ordered structures. The free energy calculations allowed us to construct phase diagrams for diblock copolymers with different polydispersity. Furthermore, an analysis of the free energy provides an understanding of the mechanism of structural change.

Theoretical Framework

A. Polydispersity Model. For an ensemble of n_c polydisperse polymers, each polymer chain can be classified by an index i. In the current study, the polydispersity originates from the molecular weight distribution, thus each chain is uniquely characterized by its molecular weight or, equivalently, its length. For each polymer of type i, the chain length is specified as $N(i)$, and there are n_i of i-type polymer chains in the ensemble. For the polydisperse polymer systems the average chain length is given by

$$\bar{N} = \sum_i N(i)\left(\frac{n_i}{n_c}\right) \tag{1}$$

The normalized chain length of the ith-type polymer is $\sigma_i = N(i)/\bar{N}$, where $\bar{N}$ is the average chain length. Since we are only considering polydispersity in terms of polymer chain length, we can use σ_i as the unique index for each type (and drop the i subscript). Furthermore, assuming a continuous distribution, a probability distribution, $p(\sigma) = n_\sigma/n_c$, can be defined. In terms of the probability distribution, the average of any function $f(\sigma)$ is defined as

$$\langle f(\sigma)\rangle = \int_0^\infty f(\sigma)p(\sigma)\,\mathrm{d}\sigma \tag{2}$$

By definition, $\langle\sigma\rangle = 1$. The weight-averaged and number-averaged chain lengths (which are proportional to the weight-averaged and number-averaged molecular weights) are given by

$$M_w = \frac{\langle N(\sigma)^2\rangle}{\langle N(\sigma)\rangle} = \bar{N}\langle\sigma^2\rangle,\ M_n = \langle N(\sigma)\rangle = \bar{N} \tag{3}$$

The polydispersity index PDI $= M_w/M_n$ can be shown to be ≥ 1. In what follows we will use a related parameter

$$\kappa = \frac{M_w}{M_n} - 1 = \langle(\sigma - 1)^2\rangle \tag{4}$$

to characterize the polydispersity. We will take the advantage that, for narrow molecular weight distributions, κ is a small number. Therefore, a perturbation method can be developed by treating κ as a perturbative parameter. It is also noticed that κ is the variance of the distribution $p(\sigma)$. Experimentally, a "nearly monodisperse" polymer melt will have κ in the range 0−0.05. For many synthetic polymers, a realistic model of the molecular weight distribution is the Schulz−Zimm (or gamma) distribution, which is defined as

$$p(\sigma) = \frac{k^k}{\Gamma(k)}\sigma^{k-1}\mathrm{e}^{-k\sigma} \tag{5}$$

For the Schultz−Zimm distribution, the polydispersity parameter is $\kappa = 1/k$.

Since a diblock copolymer chain is composed of two different subchains, it is necessary to consider two distributions, one for each block. The α-type block is specified by an average block length $\bar{N}_\alpha$ (Greek letters will be used to label blocks), and a probability distribution $p_\alpha(\sigma_\alpha)$. During the production of the diblock copolymers, the polymerization of one block is usually insensitive to the polymerization of the other block. Therefore, the distributions for the two blocks can be considered as independent distributions. Hence, the overall molecular weight distribution $p_{AB}(\sigma_A,\sigma_B)$ is given by the product of the block distributions

$$p_{AB}(\sigma_A,\sigma_B) = p_A(\sigma_A)p_B(\sigma_B) \tag{6}$$

and the average of any function $f(\sigma_A,\sigma_B)$ is given by

$$\langle f(\sigma_A,\sigma_B)\rangle_{AB} = \int\int f(\sigma_A,\sigma_B)p_A(\sigma_A)p_B(\sigma_B)\,d\sigma_A\,d\sigma_B \quad (7)$$

The independence of the block distributions lead to the simple result that

$$\langle f(\sigma_A)g(\sigma_B)\rangle_{AB} = \langle f(\sigma_A)\rangle_A\langle g(\sigma_B)\rangle_B \quad (8)$$

For a given type, $\sigma \equiv (\sigma_A,\sigma_B)$, of the copolymers, the chain length is specified as $N(\sigma) = \bar{N}_A\sigma_A + \bar{N}_B\sigma_B$, and the average copolymer chain length is $\bar{N} = \bar{N}_A + \bar{N}_B$. The polydispersity parameters of the individual blocks are then given by the averages $\kappa_\alpha = \langle(\sigma_\alpha - 1)^2\rangle_{AB}$. The overall polydispersity parameter of the diblock copolymer chains will be given by the rule for the sum of variances of statistical distributions

$$\kappa = f_A^{\,2}\kappa_A + f_B^{\,2}\kappa_B \quad (9)$$

where $f_\alpha = \bar{N}_\alpha/\bar{N}$ is the average fraction of the α-block. It should be noted that, in general, $\bar{N}_\alpha/\bar{N} \neq \langle N_\alpha/N\rangle$.

For narrow molecular weight distributions, the evaluation of the averages in (7) can be approximated by a Taylor series expansion about $\sigma = 1$. To the second order of the variable $(\sigma - 1)^2$, the average is given by

$$\langle f(\sigma_A,\sigma_B)\rangle_{AB} \approx f(1,1) + \frac{1}{2}\sum_\alpha \kappa_\alpha \frac{\partial^2 f}{\partial\sigma_\alpha^{\,2}}\bigg|_{\sigma_A=\sigma_B=1} \quad (10)$$

The above approximate evaluation of the integrals is equivalent to a molecular weight distribution of the form

$$p_\alpha(\sigma_\alpha) = \delta(\sigma_\alpha - 1) + \frac{1}{2}\kappa_\alpha\delta''(\sigma_\alpha - 1) \quad (11)$$

where $\delta''(x)$ is the second derivative of the Dirac δ function $\delta(x)$.

In the studies by Fredrickson and Sides,[15] it was assumed that $p_A(\sigma_A) = \delta(\sigma_A - 1)$ and a Schulz−Zimm distribution for $p_B(\sigma_B)$ was used. The integral in (7) was evaluated using Gaussian quadrature. Their method has the advantage of being more accurate at larger κ_α. In what follows we will use the perturbative method (eq 10) to evaluate the integrals over the molecular weight distributions. Therefore, the results presented in this paper will be restricted to narrow molecular weight distributions.

B. Self-Consistent Mean-Field Theory. The self-consistent field theory for polydisperse block copolymers can be derived most conveniently using the formalism given by Schmid,[20] which considers melts of multiple polymer types. For a canonical ensemble n_c polymer chains, of which n_σ are of type σ, are contained in a volume V. It is convenient to view a polydisperse polymer system as a polymer blend composed of polymers with different molecular weights. For simplicity, the volume occupied by each monomer is assumed to be the same for the A and B blocks, $v_A = v_B = v_0$, so that the volume of a σ-type polymer is $N_\sigma v_0$. The probability distribution of chain length is given by $p(\sigma) = n_\sigma/n_c$. Each polymer chain is modeled by a Gaussian chain. Specifically, the ith polymer chain of type σ is represented by a space curve $R_{\sigma,i}(s)$, where $0 \le s \le N_\sigma$ is the arc-length parameter and $N_\sigma = \bar{N}_A\sigma_A + \bar{N}_B\sigma_B$ is the length of the polymer chain. Following Schmid, we define a structure−function $\gamma_{\alpha j}(s)$ which is 1 when $R_{\sigma,i}(s)$ is an α-monomer and 0 otherwise. For diblock copolymers, $\gamma_{\alpha j}(s) = \delta_{\alpha,A}$ when $0 \le s < N_{A,j}$, and $\delta_{\alpha,B}$ when $N_{A,j} < s \le N_j$. In the following, however, we will scale s by the average polymer length: $t = s/\bar{N}$. The interaction between the different blocks is assumed to be described by an effective short-range potential characterized by a Flory−Huggins parameter χ.

Starting from the partition function of the polymer chains, the derivation of SCFT equations for polydisperse polymers follows the theory of Fredrickson and Sides.[14,15] For the model system adopted in the current study and within the mean-field approximation, the statistics of the polymers is modeled by one independent polymer chain in a set of effective chemical potential fields $\omega_\alpha(\mathbf{r})$. These chemical potential fields are conjugate to the monomer density fields $\phi_\alpha(\mathbf{r})$. In terms of these mesoscopic variables, the free energy per chain of the block copolymer melt is given by

$$f \equiv \frac{F\bar{N}v_0}{Vk_BT} = \frac{1}{V}\int d\mathbf{r}\,\{\chi\bar{N}\phi_A(\mathbf{r})\phi_B(\mathbf{r}) - \sum_\alpha \omega_\alpha(\mathbf{r})\phi_\alpha(\mathbf{r})\} - \langle \ln Q_\sigma\{\omega_\alpha\}\rangle_{AB} \quad (12)$$

where $Q_\sigma(\{\omega_\alpha\})$ is the partition function of a single type-σ diblock copolymer chain in the chemical potential fields $\omega_\alpha(\mathbf{r})$. This single-chain partition function can be expressed in terms of the end-integrated propagators, $q_\sigma(\mathbf{r},t)$, which are solutions of the modified diffusion equations

$$\frac{\partial}{\partial t}q_\sigma(\mathbf{r},t) = \sum_\alpha \gamma_{\alpha\sigma}(t)\left[\frac{\bar{N}b_\alpha^{\,2}}{6}\nabla^2 - \omega_\alpha(\mathbf{r})\right]q_\sigma(\mathbf{r},t) \quad (13)$$

with the initial conditions $q_\sigma(\mathbf{r},0) = 1$. In terms of the end-integrated propagator $q_\sigma(\mathbf{r},t)$, the single-chain partition function is

$$Q_\sigma = \frac{1}{V}\int d\mathbf{r}\, q_\sigma(\mathbf{r}, N_\sigma/\bar{N}) \quad (14)$$

In addition, we define a conjugate end-integrated propagator, $q_\sigma^\dagger(\mathbf{r},t)$, which satisfies the same differential equation as $q_\sigma(\mathbf{r},t)$, but with a different initial condition $q_\sigma^\dagger(\mathbf{r},1) = 1$. From the expression of the free energy density, it can be seen that the polydispersity effect on the diblock copolymers is contained in the last term of (12), which is an average of the logarithm of the single-chain partition function, $-\langle \ln Q_\sigma\{\omega_\alpha\}\rangle_{AB}$.

Within the mean-field approximation, the SCFT equations determining the polymer densities $\phi_\alpha(\mathbf{r})$ and chemical potential fields $\omega_\alpha(\mathbf{r})$ are obtained by minimizing the free energy, subjected to the incompressibility condition. Specifically the SCFT equations are given by

$$\omega_A(\mathbf{r}) = \chi\bar{N}\phi_B(\mathbf{r}) + \xi(\mathbf{r}) \quad (15)$$

$$\omega_B(\mathbf{r}) = \chi\bar{N}\phi_A(\mathbf{r}) + \xi(\mathbf{r}) \quad (16)$$

$$\phi_\alpha(\mathbf{r}) = -V\left\langle\frac{\delta \ln Q_\sigma}{\delta\omega_\alpha(\mathbf{r})}\right\rangle_{AB} \quad (17)$$

where the function $\xi(\mathbf{r})$ is a Lagrangian multiplier to ensure the incompressibility condition $\phi_A(\mathbf{r}) + \phi_B(\mathbf{r}) = 1$. In terms of the propagators, the polymer densities can be written as

$$\phi_\alpha(\mathbf{r}) = -\left\langle\frac{1}{Q_\sigma}\int dt\,\gamma_{\alpha\sigma}(t)q_\sigma(\mathbf{r},t)q^\dagger{}_\sigma(\mathbf{r},t)\right\rangle_{AB} \quad (18)$$

For a given set of controlling parameters, $\{\chi\bar{N}, N_\alpha, p_\alpha(\sigma)\}$, the SCFT equations must be solved to obtain solutions for different ordered structures. The free energies of the different

structures are then used to construct the phase diagram. The technique of solving the SCFT equations is similar to the one used for monodisperse polymers. The only added complication comes from the averaging over the molecular weight distributions. In the studies of Fredrickson and Sides,[14,15] the SCFT equations are solved in real-space and the averages over the molecular weight distributions were carried out using the Gaussian quadrature method. This real-space method for polydisperse block copolymers has been extended to the study of vesicle formations in dilute diblock copolymer solutions by Jiang et al.[21] While the real-space method provides an efficient method to search for ordered structures, the reciprocal-space method can be used to obtain accurate solutions for known ordered structures. In this paper we solve the SCFT equations using the reciprocal-space method. Furthermore, a perturbation theory is used to carry out the averages over the molecular weight distributions. Details of the reciprocal methods and perturbation theory are given in Appendices A and B.

In general, the SCFT equation (eq 15) cannot be solved exactly. A variety of numerical methods have been developed to find solutions of the SCFT equations. For ordered structures, Matsen and Schick[8] invented an efficient method which utilizes the symmetry properties of the phases. The essence of the method is to restrict the function space to a smaller one with the desired symmetry. Specifically, a set of basis functions $f_n(\mathbf{r})$ is used to span the function space. The basis functions are chosen as the eigenfunctions of the Laplace operator, $\nabla^2 f_n(\mathbf{r}) = -\lambda_n f_n(\mathbf{r})$, with appropriate boundary conditions consistent with the symmetry of the ordered phase under investigation. Here λ_n is the eigenvalue corresponding to $f_n(\mathbf{r})$. An arbitrary function with the symmetry of the ordered phase can be expanded as

$$g(\mathbf{r}) = \sum_{n=1}^{\infty} g_n f_n(\mathbf{r}) \tag{19}$$

In terms of the expansion coefficients, the SCFT equations become a set of nonlinear algebraic equations. An efficient method based on matrix manipulations can be used to find solutions. Details of the reciprocal method have appeared in several publications.[5,8]

Extension of the SCFT to polydisperse diblock copolymers requires the averages of ln Q and $(\delta \ln Q)/\delta\omega_\alpha$ over the molecular weight distributions. The perturbative expansions of ln Q is given by

$$\langle \ln Q \rangle_{AB} = \ln Q + \frac{1}{2}\sum_{\alpha=A,B} \kappa_\alpha \left[\frac{1}{Q}\frac{\partial^2 Q}{\partial \sigma_\alpha^{\,2}} - \frac{1}{Q^2}\left(\frac{\partial Q}{\partial \sigma_\alpha}\right)^2 \right] \tag{20}$$

where the terms on the right-hand side are evaluated at $\sigma_A = \sigma_B = 1$. The average over the functions $(\delta \ln Q)/\delta\omega_\alpha$ can be calculated in a similar fashion. Once $\phi_\alpha = -V\langle 1/Q\ \delta Q/\delta\omega_\alpha\rangle_{AB}$ and $\langle \ln Q\rangle_{AB}$ have been calculated, the SCFT calculation proceeds just as in the monodisperse melt.

C. Random Phase Approximation. At a high temperature or small $\chi\bar{N}$, the block copolymers are in a disordered state. The transition from the disordered state to an ordered state can be studied by analyzing the two-body correlation function, or equivalently, the scattering function, of the system.[11] Specifically, the spinodal point of the disordered state occurs when the correlation function becomes zero, or the scattering function approaches infinity. In the disordered state, the scattering function for a polydisperse diblock copolymer melt can be derived using a random phase approximation (RPA). RPA analysis of polydisperse diblock copolymers has been carried out by Hong and Noolandi[12] using a model in which the A and B block molecular weight distributions are correlated. Leibler and Benoit[11] performed a similar analysis using a different averaging procedure. Burger et al.[13] have derived a Landau-type theory for polydisperse diblock copolymers using RPA and uncorrelated blocks. More recently, Sides and Fredrickson[15] have implemented continuous polydispersity in the RPA theory, and compared the RPA theory with the SCFT calculations. The RPA scattering function for a polydisperse diblock copolymer melt is reproduced here for completeness and, more importantly, for a validation of the perturbation theory used in the current study. In particular, the RPA scattering function evaluated using the perturbative expansion (eq 11) is compared with that using the full Schulz−Zimm distribution (eq 5). Details of the RPA scattering function are given in Appendix A.

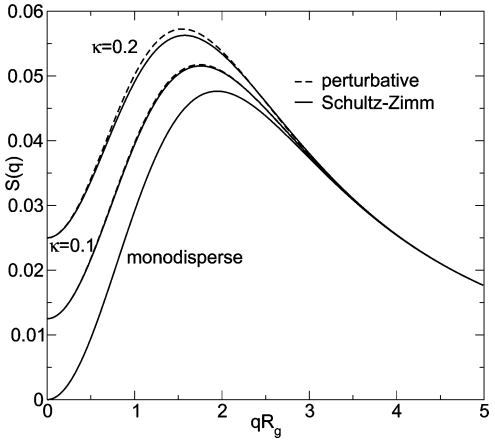

Figure 1. Structure−function as determined from the RPA, plotted vs q. The figure is for $f_A = f_B = 0.5$, with three different symmetric ($\kappa = \kappa_A = \kappa_B$) polydispersity distributions: monodisperse, perturbative, and Schultz−Zimm.

For a symmetrically polydisperse diblock copolymer melt ($\kappa_A = \kappa_B = \kappa$), Figure 1 shows the strcuture function as a function of qR_g for different values of κ. The essential feature of the scattering function, i.e., a peak at a finite q, is maintained for polydisperse diblock copolymer melts. Furthermore, it can be observed from this plot that the difference between the perturbative and the Schulz−Zimm distributions are indistinguishable for $\kappa_A = \kappa_B = 0.1$, and only slightly greater for $\kappa_A = \kappa_B = 0.2$. For a symmetric diblock melt, $f_A = 0.5$, the critical value of the wave vector q^* and the ODT point χN_c are shown in Figure 2 as functions of κ. It is noticed that the differences between the full Schulz−Zimm distribution and the perturbation result are minor up until $\kappa = 0.4$ for the critical wave vector q^*, and up until $\kappa = 0.2$ for the critical value of χN. This suggests that the perturbative distribution is a good approximation to the Schulz−Zimm distribution for narrow molecular weight distributions. Furthermore, Figure 2 demonstrates that the critical wave vector q^* is a decreasing function of κ, indicating that polydispersity results in a larger domain spacing. The ODT point χN_c is a decreasing function of κ, thus polydispersity will lead to an increase in the transition temperature (a decrease in the value of χN at the transition). All these features are confirmed in the SCFT calculations.

Results and Discussions

A. Phase Diagrams. For a given set of parameters $\{\chi N, f_A, \kappa_A, \kappa_B\}$, the phase diagram can be constructed by comparing the free energy of different ordered structures. In the reciprocal-space method, the ordered structures being considered are chosen according to experimental studies and/or real-space calculations.

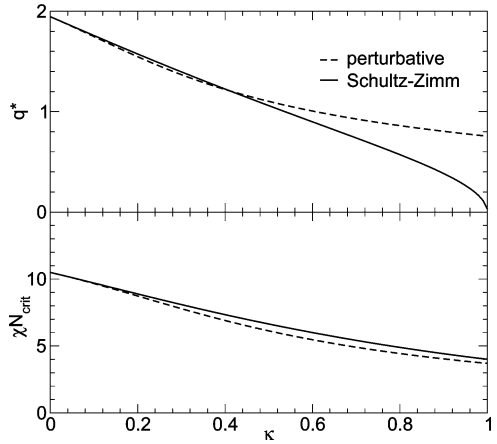

Figure 2. Position of divergence in scattering function as a function of the polydispersity ($\kappa = \kappa_A = \kappa_B$) at $f_A = f_B = 0.5$. Top graph is the critical wave vector q^*; bottom graph is the critical value of χN. For $\kappa < 0.4$, the perturbation model of polydispersity and the Schultz−Zimm model agree closely. At $\kappa = 1$ (PDI = 2), the Schultz−Zimm model predicts macrophase separation at $\chi N_{crit} = 4$, which has not been observed.[18]

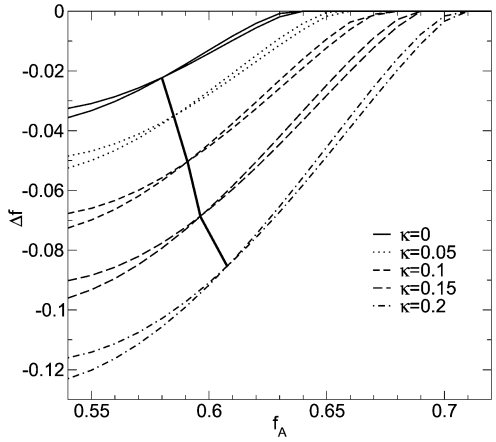

Figure 3. Free energy density of the cylindrical and gyroid phases at a fixed $\chi N = 12$ and different $\kappa = \kappa_A = \kappa_B$. The thick solid line that intersects the free energies denotes the boundary between the C and G phases for each value of κ.

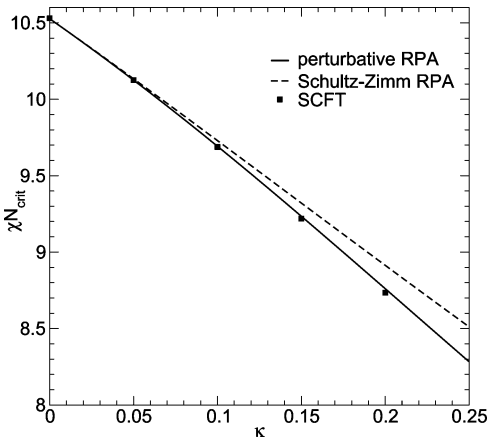

Figure 4. Comparison of the SCFT ODT point to the RPA spinodal line for $f = 0.48$.

Unlike the real-space method used by Fredrickson and Sides,[14,15] the symmetries of the structures (i.e. the space group) is chosen a priori. For the case of diblock copolymer melts, the stable structures include lamellar (L), hexagonally packed cylinders (C), bicontinuous gyroid (G), and body-centered cubic spheres (S). Within the perturbation theory, the polydispersity must be small, thus the possibility for new structures besides these four phases is not considered here. Because the face-centered cubic spherical phase is an unstable structure for diblock copolymers,[29] it is not included in our calculations. In addition, phase coexistence is also ignored, as experimentally phase separation is not observed at low polydispersities.[26] At a given point in the phase space, the free energy of these four structures are computed, and the phase with the lowest free energy is taken as the equilibrium phase.

Because the free energy difference between the different ordered structures is small, accurate calculations of the free energy is required for the determination of phase boundaries. One of the advantages of the reciprocal-space method is that it enables accurate free energy computations. As an example of the free energy calculation and phase boundary determination, the calculated free energy of the C and G structures for a fixed $\chi N = 12$ and different polydispersity parameters is plotted as a function of f_A in Figure 3. Phase boundary between these two structures is determined by the intersect of the free energies. It is clear from this figure that polydispersity has a significant effect on the phase boundary, and increasing the polydispersity leads to a shift of the G−C phase boundary farther away from $f_A = {}^1/_2$.

A possible test of the accuracy of the perturbation theory used in the current study is to compare the phase boundary between the spherical and homogeneous phases with the spinodal line of the homogeneous phase calculated from the RPA (eq A1). These two boundaries should coincide at the critical point $f_A = 0.5$, and they should be close to each other for values of f_A near 0.5. Ideally we should use the critical point to make the comparison. However, at the critical point the convergence of the SCFT solutions becomes very slow, and extrapolation must be used as the free energy can only be determined within the ordered regime. In addition, the extrapolation (using a parabolic fit) becomes singular at the critical point, as the first derivative of the free energy is continuous and zero there. Because of these problems associated with the critical point SCFT calculations, the ordered-disorder transition (ODT) point for $f_A = 0.48$ is chosen to make the comparison. The computed ODT boundary for $f_A = 0.48$ is shown in Figure 4. This value of f_A is sufficiently far away from the critical point for results to be accurately determined, yet close enough to be useful for comparison. The result shows that the RPA spinodal point is in excellent agreement with the ODT determined from perturbative SCFT for small values of $\kappa < 0.1$.

From the computed free energy for the different phases, phase diagrams in the $\chi\bar{N} - f_A$ space can be constructed for different molecular weight distributions. In what follows, phase diagrams for polydisperse diblock copolymers with symmetric molecular weight distributions ($\kappa_A = \kappa_B = 0.05, 0.15$) as well as asymmetric molecular weight distributions ($\kappa_B = 0$ and $\kappa_A = 0.05$ and 0.15) are presented. In Figure 5, phase diagrams for diblock copolymer melts with equal polydispersities in the A and B blocks are shown, along with the phase diagram for the monodisperse diblock copolymer melt. The phase diagrams are symmetric about $f_A = 0.5$ and parabolic. The triple points are at the intersection of the C, G and L phases, and there is a critical point at $f_c = 0.5$. These features are the same as the monodisperse diblock copolymer melt. The most striking change in the phase diagram is a decrease in the order−disorder transition point to a smaller χN, and a corresponding displacement in the other phase transition boundaries. The decrease of the ODT point is predicted by the RPA and the SCFT results are in quantitative agreement with the RPA prediction. Furthermore, for a fixed value of χN (e.g., $\chi N = 15$ for Figure 5) the stable region of

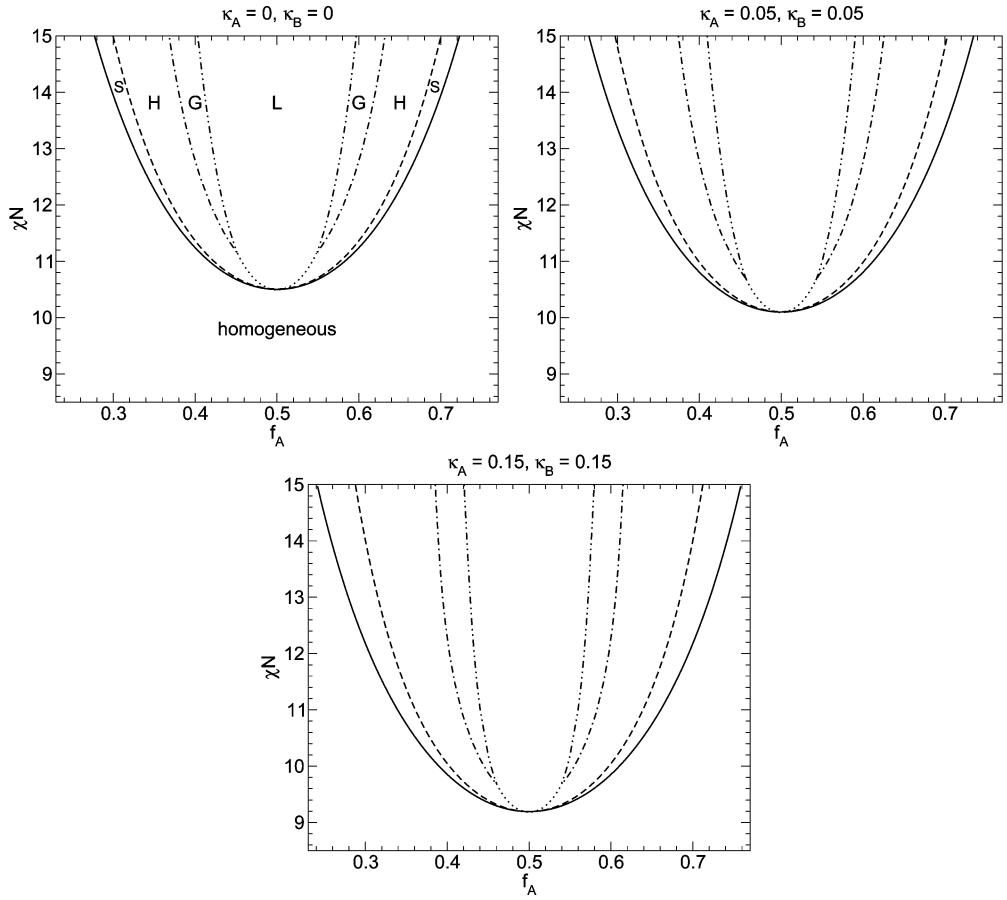

Figure 5. Phase diagrams for symmetrically diblock copolymer melts. For a given value of $\chi\bar{N}$, the phase transition sequence is the same as that of the monodisperse melt.

the lamellar phase decreases as κ increases, while the stable region of the cylindrical phase increases. This preference for the cylindrical morphology is consistent with experimental observations at moderate polydispersities.[26] As κ increases, the L−G and G−C phase boundaries become less parabolic and closer to being constant for large χN, which accounts for the lack of broadening at $\chi N = 15$, compared with the broadening at $\chi N = 12$ in Figure 3. In addition, the width of the G region remains about the same. Although not clear from Figure 5, the position of the ODT at different values of f_A follows the same linear relationship with respect to κ as the critical point does in Figure 4. The ODT boundary can be obtained by shifting the ODT boundary of a monodisperse diblock copolymer melt using an effective average block length $\tilde{N} \approx (1 + 0.8\kappa)N$ (at low polydispersity). This would suggest that a measure of chain length in between the number average and the weight average would be more appropriate for the ODT. However, the order−order transition lines do not follow this simple scaling, reflecting the fact that these transitions are driven by a delicate balance between the energy and entropy of the polymer chains.

In general, the two blocks have different molecular weight distributions due to the different reaction rates of the polymers. Therefore, phase diagrams for asymmetrically polydisperse diblock copolymers are of great interest. As an example of asymmetrically polydisperse diblock copolymers, the one-sided polydisperse diblock copolymers $\kappa_B = 0$ are considered. Phase diagrams for one-sided polydisperse diblock copolymer melts with $\kappa_A = 0.05$, and $\kappa_A = 0.15$ are shown in Figure 6. The first feature to be noticed from these phase diagrams is that the polydispersity asymmetry breaks the $f_A \leftrightarrow 1 - f_A$ symmetry of the phase diagram. The phase boundaries are still roughly parabolic, albeit no longer symmetrical about $f_A = 0.5$. The critical point has moved up one side of the ODT, instead of being at the minimum χN of the ODT. This is mirrored by the shift of the triple points, which are tilted with respect to their monodisperse positions. The regions of stability have changed also. The phases with the polydisperse blocks in the minority domains occupy a wider range of f_A for a given χN, while the region of those phases with the polydisperse blocks in the majority domains become smaller. The decrease in the ODT point is approximately the same as that for a symmetric polydisperse melt with $\kappa_{sym} = 1/2\ (\kappa_A + \kappa_B)$, implying that the amount of decrease is due to the average of the block polydispersities.

For monodisperse diblock copolymer melts, the $f_A \leftrightarrow 1 - f_A$ symmetry of the phase diagram originates from the assumption of equal Kuhn lengths of the two blocks. Matsen and Schick have shown that conformational asymmetry or unequal Kuhn length will break this symmetry of the phase diagram.[23] The phase diagrams presented in this section demonstrate that different molecular weight distributions can also lead to asymmetric phase diagrams for polydisperse diblock copolymer melts. It is interesting to note that the phase diagrams for the asymmetrically polydisperse diblock copolymers have the same features as the phase diagrams for conformationally asymmetric diblock copolymers. In particular, the blocks with a broader molecular weight distribution corresponds to a larger Kuhn length.

B. Domain Spacing. Besides the shift of the phase boundaries and the breaking of the $f_A \leftrightarrow 1 - f_A$ symmetry of the phase diagram, polydispersity has a pronounced effect on the domain spacing of the ordered structures. Specifically, it has been

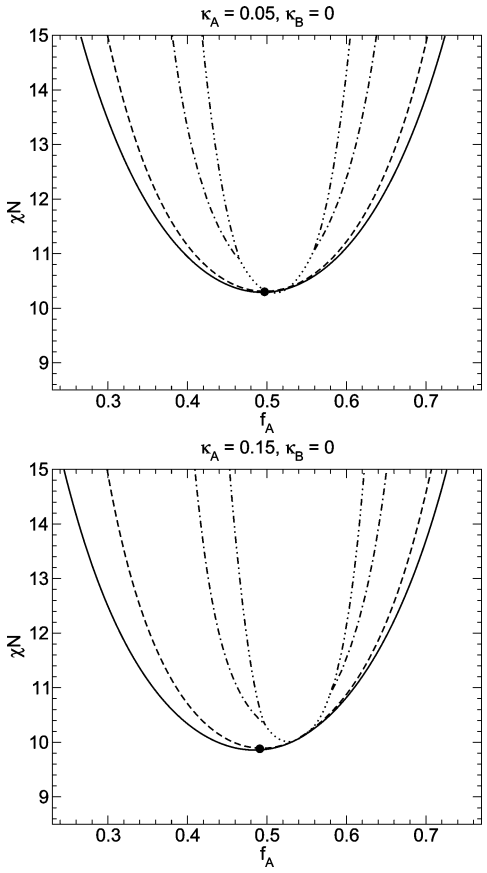

Figure 6. Phase diagrams for diblock melts with the A block polydisperse, and the B block monodisperse. The dot (●) is the position of the RPA critical point.

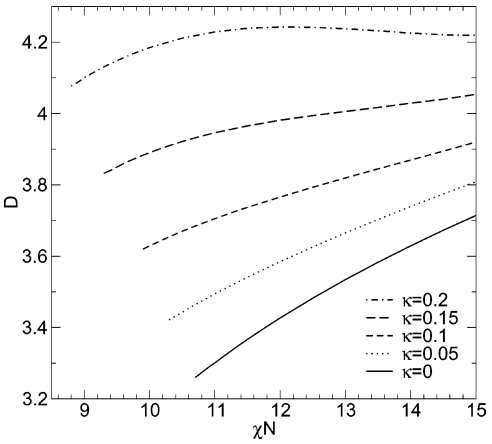

Figure 7. Period of the lamellar phase for $f_A = 0.5$ and $\kappa = \kappa_A = \kappa_B$.

predicted by the RPA analysis and SCFT that polydispersity leads to larger domain spacings or periods as compared with an equivalent monodisperse block copolymers. As an example of this effect, the period of the lamellar phase with $f_A = 0.5$ and different polydispersity parameters is plotted as a function of $\chi\bar{N}$ in Figure 7. The increase of the domain spacings with polydispersity is obvious in this plot. Another observation is that the slope of change in the domain spacing is smaller for larger κ. Experimentally, the effect on domain spacing should be easier to observe than the phase boundary shifts, as the domain spacing is given by scattering techniques and/or by direct observation with microscopy. Since $\chi\bar{N}$ is approximately proportional to the inverse of the temperature, this effect can be examined by analyzing the domain spacing as a function of temperature.

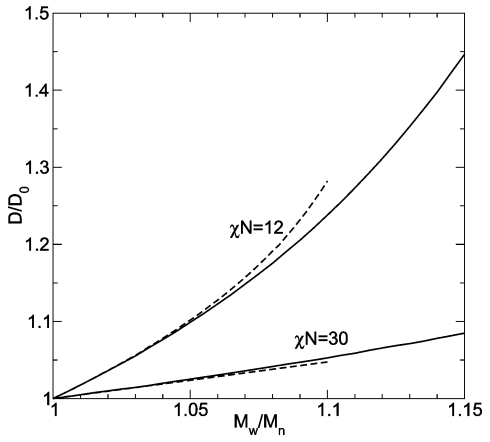

Figure 8. Comparison of D/D_0 values for a lamellar system, with $f_A = 0.5$, at two different $\chi\bar{N}$ values. M_w/M_n is the polydispersity of the whole chain (eq 9). The dashed lines are for systems with a polydisperse A block, and a monodisperse B block (so $M_w/M_n = 1 + \kappa_A/4$), and the solid lines are for systems where both blocks are equally polydisperse (where $M_w/M_n = 1 + (\kappa_A + \kappa_B)/4$).

The increase of the domain spacing with polydispersity is demonstrated more directly in a plot of the period as a function of the polydispersity index. One example is shown in Figure 8 for the lamellae with $f_A = 0.5$ and different values of $\chi\bar{N}$. For small values of κ, the domain spacing increases linearly with the polydispersity index. This linear behavior is consistent with the experimental results of Noro et al.[17] in the small κ region. Linear increase of the domain spacing has also been reported by Lynd and Hillmyer.[19] However the experiments of Lynd and Hillmyer were carried out at large values of $\kappa > 0.4$. Therefore, a direct comparison between their observation and our result is not appropriate because of the perturbation theory used.

The mechanism of the domain-spacing increase can be understood based on the idea that polydisperse copolymers release part of the stretching energy of the chains. For an incompressible polymeric system, the distribution of the polymers must be adjusted to maintain a constant density. For a monodisperse melt, polymer chains will have to be stretched away from the interface and compressed close to the interface such that a constant density is achieved. For a polydisperse melt, on the other hand, the existence of long and short chains will alleviate the stretching and compression of the chains, thus reducing the entropic energy of the chains. The domain spacing is, however, dominated by the longer chains, leading to a large period.

Qualitatively, this mechanism can be justified by examining the segregation of polymer chains according to their lengths. The chain segregation is obtained by analyzing the contribution to the total polymer density from polymers with different chain lengths. By considering a nonperturbative distribution for the polydispersity (here we use the Schultz−Zimm distribution), a blend of n monodisperse polymer types can be constructed which approximates the polydisperse melt. If $[0,\infty)$ is split into intervals $[\sigma_i,\sigma_{i+1})$ such that

$$\int_{\sigma_i}^{\sigma_{i+1}} p(\sigma)\, \mathrm{d}\sigma = \frac{1}{n} \tag{21}$$

(with $\sigma_0 = 0$ and $\sigma_n = \infty$) then an average $\bar{\sigma}_i$ can be taken such that

$$n\int_{\sigma_i}^{\sigma_{i+1}} \sigma p(\sigma)\, \mathrm{d}\sigma = \bar{\sigma}_i \tag{22}$$

By taking $\bar{N}\bar{\sigma}_i$ as the length of the ith polymer type, our blend

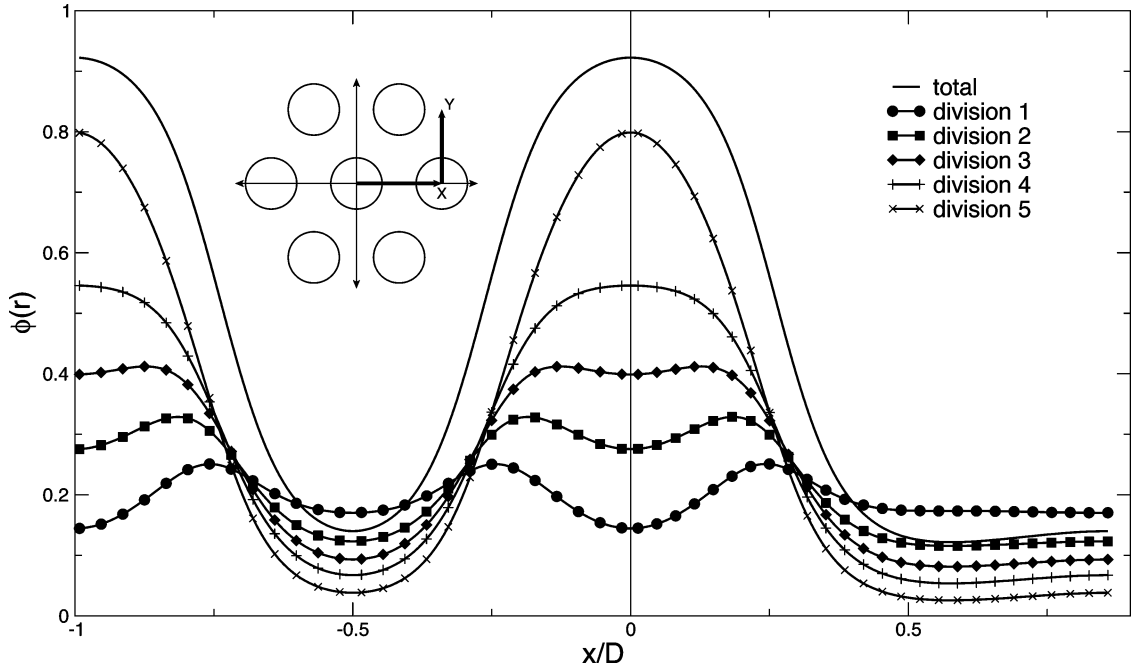

Figure 9. Volume fraction profiles for the A block of a cylindrical phase ($\chi N = 13.5$, $f_A = 0.35$,$\kappa_A = 0.2$,$\kappa_B = 0$, where the polydisperse melt is approximated using five monodisperse components.

approximates the polydisperse melt, with the advantage that each component corresponds to an equal portion of the polydispersity curve. This is similar to the technique used in ref 15, except there the polydispersity distribution was split so the integral in the average (eq 17) can be done as a Gaussian quadrature.

As an example, Figure 9 shows the profiles of the A block volume fractions when a polymer polydisperse in the A block is split into five divisions by the scheme above. A segregation of polymer chains according to their lengths can be noticed from this figure. The longer blocks preferentially occupy the center of the cylinders, whereas the shortest A blocks have a higher concentration between the cylinders. This segregation of polymer has been noticed by Sides and Fredrickson[15] and by Jiang et al.[21]

Quantitative understanding of the mechanism for the domain-spacing increase can be obtained by decomposing the free energy density into interfacial contribution and stretching contribution, as proposed by Shi and Noolandi.[24] For an ordered structure with a domain spacing D, the free energy per chain can be approximated by the following expression

$$f = f_{\text{demix}} + \frac{\gamma}{D} + \alpha D^2 \qquad (23)$$

where f_{demix} is the free energy per chain for a completely demixed melt, γ is the interfacial tension between the A and B domains, and the last term presents the stretching energy of the polymer chains. The equilibrium domain spacing is determined by the competition between the interfacial and stretching energies. An example of such a decomposition is given in Figure 10 for an one-sided polydisperse diblock copolymer with $f_A = 0.35$ and $\chi N = 13.5$. This figure shows that, for this cylinder-forming diblock copolymers, the function form gives a good description for the free energy as a function of the domain spacing. The results demonstrate that polydispersity has very little effect on the AB interfacial free energy. On the other hand, the chain stretching energy decreases as the polydispersity is increased. Since the equilibrium domain spacing is determined by the competition between the interfacial and stretching energies, the decrease of the stretching energy leads to a larger domain spacing.

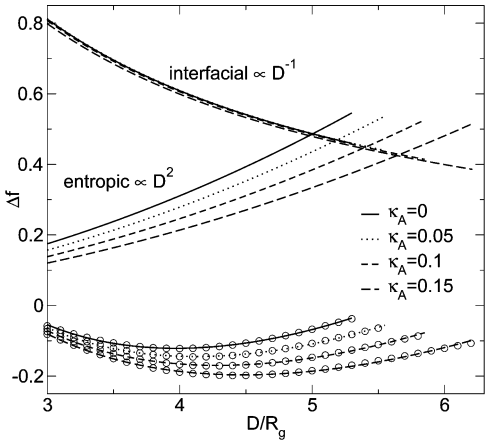

Figure 10. Decomposition of free energy into interfacial and entropic parts for a cylindrical phase with $f_A = 0.35$, $\chi N = 13.5$, and a polydisperse A block and a monodisperse B block. The circles are the free energies as calculated with the perturbation theory, and the lines connecting them are the fits using (23).

Conclusions

The phase behavior of polydisperse diblock copolymer melts are studied by using a reciprocal-space self-consistent field theory and treating the polydispersity as a perturbation. The validity of the perturbation theory is tested by comparing the SCFT results with the RPA theory. Phase diagrams for polydisperse diblock copolymer melts are constructed by examining the free energy density of different ordered structures. For symmetric molecular weight distributions of the blocks, the phase diagrams maintain the symmetry about $f_A = 0.5$, and the phase boundaries shift to smaller values of $\chi\bar{N}$. For a given value of $\chi\bar{N}$, the nonlamellar phase regions become wider at the cost of the lamellar phase. The phase boundary between the disordered and spherical phase (order−disorder line) is in good agreement with the RPA prediction. For asymmetric molecular weight distributions of the blocks, the $f_A \leftrightarrow 1 - f_A$ symmetry

of the phase diagram is broken. The phase boundaries become asymmetric about $f_A = 0.5$. The phase diagrams for the asymmetrically polydisperse diblock copolymers resemble the phase diagram of conformationally asymmetric diblock copolymers.

Besides the shift of the phase boundaries and the breaking of the $f_A \leftrightarrow 1 - f_A$ symmetry of the phase diagram, theoretical studies predict that polydispersity leads to larger domain spacing as compared with monodisperse systems. The mechanism of this domain spacing increase is that the existence of different chain lengths in a polydisperse system leads to a decrease of the stretching energy. A decomposition of the free energy density is used to illustrate this mechanism. It is shown that, while the interfacial free energy is insensitive to the polydispersity, the stretching energy decreases with large κ, resulting in a larger domain spacing.

The theoretical results from the current studies have been compared with other theoretical approaches and with available experiments. The predicted increase of the domain spacing is in agreement with all previous theoretical studies and with experiments. Because the averaging over the molecular weight distributions was carried out using a perturbation method, the phase diagrams obtained in this paper apply to polydisperse diblock copolymer melts with narrow molecular weight distributions. Typical examples are the block copolymers obtained using ionic polymerization techniques. For molecular weight distributions with large PDI, an efficient method to carry out the averages is the Gaussian quadrature method proposed by Fredrickson and Sides. A combination of the reciprocal-space approach and the Gaussian quadrature method will be a useful routine to study the phase behavior of polydisperse block copolymers with arbitrary molecular weight distributions.

Acknowledgment. The authors would like to thank Rob Wickham for very helpful discussions, and SHARCNET for computing resources. This work was supported by the Natural Sciences and Engineering Research Council (NSERC) of Canada.

Appendix A. RPA Scattering Function

The RPA scattering function or structure factor for a monodisperse homogeneous $S(q)$ melt in terms of the scattering vector q is given by the expression[22]

$$\frac{1}{S(q)} = \frac{1}{S_{inc}(q)} - 2\chi N \tag{A1}$$

where $S_{inc}(q)$ is the incompressible structure factor

$$S_{inc}(q) = \frac{S_{AA}(q)S_{BB}(q) - S_{AB}(q)^2}{S_{AA}(q) + 2S_{AB}(q) + S_{BB}(q)} \tag{A2}$$

and $S_{\alpha\beta}(q)$ are the noninteracting monomer structure factors for a single Gaussian chain. The $S_{\alpha\alpha}$ factors are

$$S_{\alpha\alpha}(x) = \frac{2}{(f_\alpha x)^2}[f_\alpha x + e^{-f_\alpha x} - 1] \tag{A3}$$

and the off-diagonal factor is

$$S_{AB}(x) = \frac{e^{-f_A x} - 1}{f_A x}\frac{e^{-f_B x} - 1}{f_B x} \tag{A4}$$

where $x = q^2 N b^2/6$. The most important feature is that $S_{inc}(x)$ exhibits a maximum at a finite value of x^* or q^*, indicating a spontaneous selection of a length scale. For small values of χN, the scattering function $S(q)$ is finite and the disordered phase is stable. The disordered phase becomes unstable when χN reaches the minimum $^1/_2 S_{inc}(x^*)$, at which point $S(q)$ diverges. The domain spacing is characterized by q^* while the ODT boundary is given by $\chi N = {}^1/_2 S_{inc}(x^*)$.

For a polydisperse diblock copolymer melt, the individual monomer structure factors should be averaged using a weighted average:[13] $S_{\alpha\beta}(q;f_\gamma)$ is replaced with $\langle f_\alpha \sigma_\alpha f_\beta \sigma_\beta S_{\alpha\beta}(q;f_\gamma\sigma_\gamma)\rangle_{AB}$. For the model system with independent molecular weight distributions for the A and B blocks, this is equivalent to replacing $e^{-f_\alpha x}$ with $\langle e^{-f_\alpha \sigma_\alpha x}\rangle_\alpha$, so only these later averages need to be computed. For the Schulz−Zimm distribution it is straightforward to show that

$$\langle \exp(-f_\alpha x)\rangle_\alpha = (1 + \kappa_\alpha \bar{f}_\alpha \bar{x})^{-1/\kappa_\alpha} \tag{A5}$$

On the other hand, for the perturbative distribution given in (11), the average becomes

$$\langle \exp(-f_\alpha x)\rangle_\alpha = \exp(-\bar{f}_\alpha \bar{x})\left(1 + \frac{1}{2}\kappa_\alpha \bar{f}_\alpha^{\,2}\right) \tag{A6}$$

Appendix B. Spectral Solution to SCFT Equations

The SCFT equation (eq 15) cannot be solved exactly in general. One stumbling block to the solution is that the solution is a function of the position $\boldsymbol{r}$. By an appropriate discretization, eq 15 can be converted to a (large) set of coupled nonlinear equations of scalar variables. Solving the set of equations would, in principle, result in solutions of the ordered structure. However, directly solving the SCFT equations in real space is still a formidable task. For ordered structures, there is an efficient method, invented by Matsen and Schick,[8] which utilizes the symmetrical properties of the phases. The solutions that we are seeking are periodic, since we are looking for ordered phases, which suggests an expansion in a Fourier-like series. The appropriate basis functions for the expansion are the eigenfunctions $f_n(\boldsymbol{r})$ of the Laplace operator $\nabla^2 f_n(\boldsymbol{r}) = -\lambda_n f_n(\boldsymbol{r})$, where λ_n is the eigenvalue corresponding to $f_n(\boldsymbol{r})$, and with periodic boundary condition where the period is that of the unit cell of the structure being considered. The symmetries of the phase being considered will lead to degeneracies in the basis functions.

In all of the structures studied here (L, C, S, and G), only one parameter D is required to describe the period of the structure. In this case, $\lambda_n \propto 1/D^2$. In general, λ_n is the length of a reciprocal lattice vector associated with the basis function $f_n(\boldsymbol{r})$. For an orthogonal, cubic, basis, $\lambda_n = (2\pi/D)^2(h^2 + k^2 + l^2)$, and for the hexagonal, $(2\pi/D)^2(h^2 - hk + k^2)$, where (h, k, l) are the Miller indices of the related reciprocal lattice vector.

By convention, $f_0(\boldsymbol{r}) = 1$, and the eigenfunctions are ordered by increasing values of λ_n. In addition, they are taken to be orthonormal, so

$$\int d\boldsymbol{r}\, f_n(\boldsymbol{r}) f_m(\boldsymbol{r}) = \delta_{nm} \tag{B1}$$

An arbitrary function with the period of the unit cell can then be expanded in a Fourier-like series

$$g(\boldsymbol{r}) = \sum_n g_n f_n(\boldsymbol{r}). \tag{B2}$$

If block-specific end-integrated propagators

$$q_\sigma(\boldsymbol{r}, t) = \begin{cases} q_{A\sigma}(\mathrm{r}, t) & t \le h_A \\ q_{B\sigma}(\mathrm{r}, t) & t > h_A \end{cases} \tag{B3}$$

$$q_\sigma^\dagger(\boldsymbol{r}, t) = \begin{cases} q_{B\sigma}{}^\dagger(\mathrm{r}, t) & t \le h_B \\ q_{A\sigma}{}^\dagger(\mathrm{r}, t) & t > h_A \end{cases} \tag{B4}$$

are defined (with $h_\alpha = f_\alpha \sigma_\alpha$), the structure−function $\gamma_{\alpha\omega}(s)$ in (13) can be removed. With the operator $\mathscr{K}_\alpha \equiv \bar{N} b_\alpha{}^2/6\nabla^2 - \omega_\alpha(\boldsymbol{r})$, $\partial q_{\alpha\sigma}(\mathrm{r}, t)/\partial t = \mathscr{K}_\alpha q_{\alpha\sigma}(\mathrm{r}, t)$, with initial conditions

$$q_A(\boldsymbol{r}, 0) = 1 \tag{B5}$$

$$q_B(\boldsymbol{r}, h_A) = q_A(\boldsymbol{r}, h_A) \tag{B6}$$

$$q_B{}^\dagger(\boldsymbol{r}, 0) = 1 \tag{B7}$$

$$q_A{}^\dagger(\boldsymbol{r}, h_B) = q_B{}^\dagger(\boldsymbol{r}, h_B) \tag{B8}$$

The $q_\alpha(\boldsymbol{r}, t)$, $q_\alpha{}^\dagger(\boldsymbol{r}, t)$, and $\omega_\alpha(\boldsymbol{r})$ are then expanded as in (2) (unless otherwise noted, the subscript σ used for denoting the polymerization index will be implied). Substituting this expansion into (13) gives

$$\frac{\partial q_{\alpha n}(t)}{\partial t} = -\frac{\bar{N} b_\alpha{}^2}{6}\lambda_n q_{\alpha n}(t) - \sum_m \sum_l \omega_{\alpha l} q_{\alpha m}(t) \Gamma_{nml} \tag{B9}$$

where

$$\Gamma_{nml} = \int \mathrm{d}\boldsymbol{r}\, f_n(\boldsymbol{r}) f_m(\boldsymbol{r}) f_l(\boldsymbol{r}) \tag{B10}$$

The algebra can be made clearer by using a vector representation. Let $\boldsymbol{q}_\alpha(t) = [q_{\alpha 0}(t), q_{\alpha 1}(t), \ldots]^T$, and $\omega_\alpha = [\omega_{\alpha 0}, \omega_{\alpha 1}, \ldots]^T$. Then we can rewrite the above as

$$\frac{\partial \boldsymbol{q}_\alpha(t)}{\partial t} = \left[-\frac{\bar{N} b_\alpha{}^2}{6} D(\lambda) - \Omega_\alpha\right] \boldsymbol{q}_\alpha(t) \tag{B11}$$

where $\lambda = [\lambda_0, \lambda_1, \ldots]^T$, $D(\boldsymbol{x})$ is an operator that forms a matrix with $\boldsymbol{x}$ on the diagonal (and is zero everywhere else), and

$$[\Omega_\alpha]_{nm} = \sum_l \omega_{\alpha l} \Gamma_{nml} \tag{B12}$$

The solution to (11) is then

$$\boldsymbol{q}_\alpha(t) = \mathrm{V}_\alpha D(\mathrm{e}^{\epsilon\alpha^{(t-t_0)}}) \mathrm{V}_\alpha{}^T \boldsymbol{q}_\alpha(t_0) \tag{B13}$$

where the columns of V_α are the eigenvectors of the matrix in brackets in (11), $[\epsilon^\alpha]_n$ are the corresponding eigenvalues, and the exponential is done elementwise. For simplicity, let $\boldsymbol{e} = [1, 0, 0, \ldots]^T$. This gives

$$\boldsymbol{q}_A(t) = V_A D(\mathrm{e}^{\epsilon^A t}) V_A{}^T \boldsymbol{e} \tag{B14}$$

$$\boldsymbol{q}_B(t) = V_B D(\mathrm{e}^{\epsilon^B (t-h_A)}) V_B{}^T V_A D(\mathrm{e}^{\epsilon^A h_A}) V_A{}^T \boldsymbol{e} \tag{B15}$$

$$q_A{}^\dagger(t) = V_A D(\mathrm{e}^{\epsilon^A (t-h_B)}) V_A{}^T V_B D(\mathrm{e}^{\epsilon^B h_B}) V_B{}^T \boldsymbol{e} \tag{B16}$$

$$\boldsymbol{q}_B{}^\dagger(t) = V_B D(\mathrm{e}^{\epsilon^B t}) V_B{}^T \boldsymbol{e} \tag{B17}$$

The single-chain partition function is given by (14). Expanding into basis functions gives

$$Q = \sum_n q_n(h_A + h_B) \int \mathrm{d}\boldsymbol{r}\, f_n(\boldsymbol{r}) = q_0(h_A + h_B) \tag{B18}$$

This can be rewritten in our matrix notation as $Q = \boldsymbol{e}^T \boldsymbol{q}_B(h_A + h_B)$, and hence

$$Q = \boldsymbol{e}^T V_B D(\mathrm{e}^{\epsilon^B h_B}) V_B{}^T V_A D(\mathrm{e}^{\epsilon^A h_A}) V_A{}^T \boldsymbol{e} \tag{B19}$$

which is nicely symmetric. Letting $L = V_B{}^T V_A$, and $\boldsymbol{s}_\alpha(h_\alpha) = D(\mathrm{e}^{\epsilon\alpha^h \alpha}) V_\alpha{}^T \boldsymbol{e}$, we have

$$Q = \boldsymbol{s}_B(h_B)^T L s_A(h_A) \tag{B20}$$

The functional derivatives, in terms of the single-block distributions are

$$\frac{\delta Q}{\delta \omega_A(\boldsymbol{r})} = \int_0^{h_A} \mathrm{d}t\, q_A(\boldsymbol{r}, t) q_A{}^\dagger(\mathrm{r}, h_A + h_B - t) \tag{B21}$$

$$\frac{\delta Q}{\delta \omega_B(\boldsymbol{r})} = \int_0^{h_B} \mathrm{d}t\, q_B(\mathrm{r}, h_A + h_B - t) q_B{}^\dagger(\mathrm{r}, t) \tag{B22}$$

Note that $\delta Q/\delta\omega_A$ is related to $\delta Q/\delta\omega_B$ by the transformation $A \leftrightarrow B$, $q \leftrightarrow q^\dagger$. Examining the quantity $\delta Q/\delta\omega_A$, we substitute q_A and $q_A{}^\dagger$ for their expansions, giving

$$\frac{\delta Q}{\delta \omega_A} = \sum_{n,m} \int_0^{h_A} \mathrm{d}t\, q_{An}(t) q_{Am}{}^\dagger(h_A + h_B - t) f_n(\boldsymbol{r}) f_m(\boldsymbol{r}) \tag{B23}$$

The double basis functions can be removed by multiplying by $f_l(\boldsymbol{r})$, and integrating over $\boldsymbol{r}$. This gives

$$\frac{\delta Q}{\delta \omega_A} = \sum_l [\Gamma^A(B^A)]_l f_l(\boldsymbol{r}) \tag{B24}$$

where B^A and $\Gamma^\alpha(\mathrm{M})$ are defined by

$$V_A B_{nm}{}^A V_A{}^T = \int_0^{h_A} \mathrm{d}t\, q_{An}(t) q_{Am}{}^\dagger(h - t) \tag{B25}$$

$$[\Gamma^\alpha(M)]_l = \sum_{nm} [V_\alpha M V_\alpha{}^T]_{nm} \Gamma_{nml} \tag{B26}$$

Note that $\Gamma^\alpha(\mathrm{M})$ is linear in its argument. Substituting into this the solutions for q_A and $q_A{}^\dagger$ yields

$$B^A = \int_0^{h_A} \mathrm{d}t\, D(\mathrm{e}^{\epsilon^A t}) V_A{}^T \boldsymbol{e}\boldsymbol{e}^T V_B D(\mathrm{e}^{\epsilon^B h_A}) V_B{}^T V_A D(\mathrm{e}^{\epsilon^A (h_A - t)}) \tag{B27}$$

For convenience, let

$$A^A(h_B) = V_A{}^T \boldsymbol{e}\boldsymbol{e}^T V_B D(\mathrm{e}^{\epsilon^B h_B}) \mathrm{L} = (V_A{}^T \boldsymbol{e}) \boldsymbol{s}_B(h_B)^T L$$

Define $\mathrm{A} \odot \mathrm{B}$ to be elementwise multiplication of two matrices, so $[\mathrm{A} \odot \mathrm{B}]_{ij} = A_{ij} B_{ij}$. B^A can then be rewritten using A^A as

$$B^A = \int_0^{h_A} \mathrm{d}t\, D(\mathrm{e}^{\epsilon^A t}) A^A(h_B) D(\mathrm{e}^{\epsilon^A (h_A - t)}). \tag{B28}$$

By expanding into components, it can be seen that the integral above can be rewritten as

$$B^A = \mathrm{A}^A(h_B) \odot C^A(h_A) \tag{B29}$$

where $C^A(h_A)$ is given by

$$[C^{A}(h_A)]_{ij} = \int_0^{h_A} dt\, e^{\epsilon^{A}_i t} e^{\epsilon^{A}_j (h_A - t)} = \begin{cases} \dfrac{e^{\epsilon_i^A h_A} - e^{\epsilon_j^A h_A}}{\epsilon^{A}_i - \epsilon^{A}_j}, & \epsilon_i^{A} \neq \epsilon_j^{A} \\ h_A e^{\epsilon^{A}_j h_A} & \epsilon_i^{A} = \epsilon_j^{A} \end{cases} \quad \text{(B30)}$$

Similarly,

$$B^{B} = A^{B}(h_A) \odot C^{B}(h_B) \quad \text{(B31)}$$

$$\phi_B = -\frac{1}{Q}\frac{\delta Q}{\delta \omega_B} = \frac{1}{Q}\sum_l [\Gamma^{B}(B^{B})]_l f_l(\boldsymbol{r}) \quad \text{(B32)}$$

With $\langle \Gamma^{\alpha}(B^{\alpha})/Q \rangle_{AB}$ calculated as in Appendix 8, and the SCFT equations (appropriately converted to vector form) from (15), the volume fractions ϕ_α and the fields ω_α and ξ can be solved for, following the linear iteration scheme presented in ref 25. Starting from reasonable initial conditions (say, a previously calculated profile somewhere else on the phase diagram), this can be iterated to an appropriate accuracy within about 1000 iterations (taking at most a few seconds on a modern desktop processor).

Appendix C: Perturbative Polydispersity

There are two quantities that need to be averaged when extending the previous results to include polydispersity. These are ln Q for the free energy, and $\delta \ln Q/\delta\omega_\alpha$, for the volume fraction $\phi_\alpha(\boldsymbol{r})$. Let P^{α} be the vector of coefficients of the expansion of $1/Q\delta Q/\delta\omega_\alpha = \Gamma^{\alpha}(B^{\alpha})/Q$ in terms of the basis functions $f_n(\boldsymbol{r})$.

The perturbative expansions of ln Q is

$$\langle \ln Q \rangle_{AB} = \ln Q + \frac{1}{2}\sum_{\alpha=A,B} \kappa_\alpha \left[\frac{1}{Q}\frac{\partial^2 Q}{\partial \sigma_\alpha^{\,2}} - \frac{1}{Q^2}\left(\frac{\partial Q}{\partial \sigma_\alpha}\right)^2 \right] \quad \text{(C1)}$$

where the terms on the right-hand side are evaluated at $\sigma_A = \sigma_B = 1$.

The perturbative expansions of $1/Q\ \delta Q/\delta\omega_\alpha$ is

$$\left\langle \frac{1}{Q}\Gamma^{\alpha}(B^{\alpha}) \right\rangle_{AB} = \frac{1}{Q}\Gamma^{A}(B^{A}) + \frac{1}{2}\sum_{\beta=A,B} \kappa_\beta \frac{\partial^2 \Gamma^{\alpha}(B^{\alpha})/Q}{\partial \sigma_\beta^{\,2}} \quad \text{(C2)}$$

where again the terms on the right-hand side are evaluated at $\sigma_A = \sigma_B = 1$. From the expansion of $\delta Q/\delta\omega_\alpha$ in (24) and (29), and the linearity of $\Gamma^{\alpha}(M)$, this is just

$$\left\langle \frac{1}{Q}\Gamma^{\alpha}(B^{\alpha}) \right\rangle_{AB} = \Gamma^{\alpha}\left(\frac{1}{Q}(A^{\alpha} \odot C^{\alpha}) + \frac{1}{2}\kappa_A A^{\alpha} \odot \frac{\partial^2 C^{\alpha}/Q}{\partial \sigma_A^{\,2}} + \frac{1}{2}\kappa_B \frac{\partial^2 A^{\alpha}/Q}{\partial \sigma_B^{\,2}} \odot C^{\alpha} \right) \quad \text{(C3)}$$

The quantities that need to be calculated are then Q, A^{α}, and C^{α}, and their first- and second-derivatives $\partial/\partial\sigma_\alpha$ and $\partial^2/\partial\sigma_\alpha^2$. The derivatives of A^{α} and C^{α} are trivial from their definitions, and those of Q are easily derived from (20). Note that both A^{α} and Q are expressible in terms of $s_\alpha(\sigma_\alpha)$, so only the derivatives of $s_\alpha(\sigma_\alpha)$ and $C^{\alpha}(\sigma_\alpha)$ need to be determined. Once $\phi_\alpha = -V\langle 1/Q\ \delta Q/\delta\omega_\alpha \rangle_{AB}$ and $\langle \ln Q \rangle_{AB}$ have been calculated using the above procedure, the SCFT calculation proceeds just as in the monodisperse melts.

References and Notes

(1) Bates, F. S.; Fredrickson, G. H. *Phys. Today* **1999**, *2*, *52*, 32.
(2) Hamley, I. W. *The Physics of Block Copolymers*; Oxford University Press: Oxford, U.K., 1998.
(3) Matsen, M. W.; Bates, F. S. *Macromolecules* **1996**, *29*, 7641.
(4) Matsen, M. W. *J. Phys.: Condens. Matter* **2002**, *14*, R21.
(5) Shi, A.-C. In *Developments in Block Copolymer Science and Technology*; Hamley, I., Ed.; John Wiley & Sons: New York, 2004; p 265.
(6) Edwards, S. F. *Proc. Phys. Soc.* **1965**, *85*, 613.
(7) Helfand, E. *J. Chem. Phys.* **1975**, *62*, 999. Helfand, E. *Macromolecules* **1975**, *8*, 552.
(8) Matsen, M. W.; Schick, M. *Phys. Rev. Lett.* **1994**, *72*, 2660.
(9) Dolet, F.; Fredrickson, G. H. *Phys. Rev. Lett.* **1999**, *83*, 4317. Dolet, F.; Fredrickson, G. H. *Macromolecules* **2001**, *34*, 5317.
(10) Bohbot-Raviv, Y.; Wang, Z.-G. *Phys. Rev. Lett.* **2000**, *85*, 3428.
(11) Leibler, L.; Benoit, H. *Polymer* **1981**, *22*, 195.
(12) Hong, K. M.; Noolandi, J. *Polym. Commun.* **1984**, *25*, 265.
(13) Burger, C.; Ruland, W.; Semenov, A. N. *Macromolecules* **1990**, *23*, 3339.
(14) Fredrickson, G. H.; Sides, S. W. *Macromolecules* **2003**, *36*, 5415.
(15) Sides, S. W.; Fredrickson, G. H. *J. Chem. Phys.* **2004**, *121*, 4974.
(16) Matsushita, Y.; Noro, A.; Iinuma, M.; Suzuki, J.; Ohtani, H.; Takano, A. *Macromolecules* **2003**, *36*, 8074.
(17) Noro, A.; Donghyun, C.; Takano, A.; Matsushita, Y. *Macromolecules* **2005**, *38*, 4371.
(18) Bendejacq, D.; Ponsinet, V.; Joanicot, M.; Loo, Y.-L.; Register, R. A. *Macromolecules* **2002**, *35*, 6645.
(19) Lynd, N. A.; Hillmyer, M. A. *Macromolecules* **2005**, *38*, 8803.
(20) Schmid, F. *J. Phys.: Condens. Matter* **1998**, *10*, 8105.
(21) Jiang, Y.; Chen, T.; Ye, F.; Liang, H.; Shi, A.-C. *Macromolecules* **2005**, *38*, 6710.
(22) Leibler, L. *Macromolecules* **1980**, *13*, 1602.
(23) Matsen, M. W.; Schick, M. *Macromolecules* **1994**, *27*, 4014.
(24) Shi, A.-C.; Noolandi, J. *Macromolecules* **1994**, *27*, 2936.
(25) Laradji, M.; Shi, A.-C.; Noolandi, J.; Desai, R. C. *Macromolecules* **1997**, *30*, 3242.
(26) Kane, L.; Satkowski, M. M.; Smith, S. D.; Spontak, R. J. *J. Polym. Sci., Part B* **1997**, *35*, 2653.
(27) Spontak, R. J.; Williams, M. C. *J. Polym. Sci., Part B* **1990**, *28*, 1379.
(28) Birshtein, T. M. Yu.; Liatskaya, V.; Zhulina, E. B. *Polymer* **1990**, *31*, 2185. Zhulina, E. B.; Birshtein, T. M. Yu. *Polymer* **1991**, *32*, 1299. Zhulina, E. B. Lyatskaya, V.; Birshtein, T. M. Yu.; *Polymer* **1992**, *33*, 332. Lyatskaya, V.; Zhulina, E. B.; and Birshtein, *Polymer* **1992**, *33*, 343. Birshtein, T. M. Yu.; Lyatskaya, V.; Zhulina, E. B. *Polymer* **1992**, *33*, 2750.
(29) Yamada, K.; Nonomura, M.; Saeki, A.; Ohta, T. *J. Phys.: Condens. Matter* **2005**, *17*, 4877.

MA060717S